Aperture Optimization in Emission Imaging Using Optimal LROC Observers

P. Khurd, A. Rangarajan and G. Gindi

I. Introduction

We address the problem of optimizing emission imaging systems based on task performance figures of merit (FOM). For example, one might optimize SPECT collimator properties to maximize detection of a lesion (signal) embedded in a complex patient background (though we shall address a simpler problem). In such system optimization research involving detection tasks, there is an escalatory path toward making studies more realistic. One seeks to (1) model the imaging process and data noise accurately (2) make the ensemble of possible backgrounds and signals as realistic as possible (3) make the task as realistic as possible - involving in our case localization as well as detection.

To optimize the system, we need an observer and a scalar FOM to gauge detection performance as we vary system parameters. For a host of reasons, the mathematical *ideal observer* has been used. It is optimal in several senses and can, in principle, incorporate the ever more sophisticated models needed to escalate verisimilitude as per points (1)-(3) above. The ideal observer lends itself to computer simulation and forms an upper limit on possible human observer performance.

Here, we consider a new form of ideal observer that we recently proposed [1] . It extends the detection-only task to a more realistic one of detection plus localization. We revisit an old problem in system optimization: For a planar pinhole imaging system, optimize the pinhole size to attain the best task performance. This problem was addressed by [2] and others for detection only, and here we consider what happens when a localization task is added.

II. Optimal LROC Observer

We first revisit the well-known case of an ideal observer for a 2-class (signal present? or absent?) detection problem. Let $\mathbf{b}$ be the possibly stochastic background object and $\mathbf{s}$ an additive signal (lesion). The vector $\mathbf{g}$ is the observed image. Then $p(\mathbf{g}|\mathbf{b})$ is the signal-absent likelihood and $p(\mathbf{g}|\mathbf{b}+\mathbf{s})$ the signal-present likelihood. These likelihoods can be quite complex, incorporating many of the sources of variability discussed in points (1) -(3). The likelihood ratio $t(\mathbf{g}) = \frac{p(\mathbf{g}|\mathbf{b}+\mathbf{s})}{p(\mathbf{g}|\mathbf{b})}$ is an ideal observer that delivers a scalar test statistic $t(\mathbf{g})$ which is compared to a threshold τ to decide signal-present if $t(\mathbf{g}) > \tau$ and signal absent if $t(\mathbf{g}) < \tau$. At each τ, one can calculate a true positive fraction (TPF) that is the probability of deciding signal present when it is indeed present, and a false positive fraction (FPF) that is the probability of deciding that a signal is present when it is absent. By sweeping τ, one generates the well-known ROC curve TPF vs FPF. The area under this curve, AROC, is a FOM for this 2-class detection problem. The likelihood ratio is ideal in the sense that it maximizes AROC amongst all possible observers, and is also optimal in several other senses.

G. Gindi is with the Department of Radiology, SUNY Stony Brook, NY, USA (telephone: 631-444-2539, email:gindi@clio.mil.sunysb.edu). P. Khurd is with the Department of Radiology, Univ. Pennsylvania , and A. Rangarajan is with the Department of C.I.S.E., University of Florida

If we now demand that the observer both detect *and localize* the signal, the ideal observer changes [1]. Let $\mathbf{f}$ be the object, so that $\mathbf{f} = \mathbf{b}$ for the signal-absent case. Under the signal-present hypothesis, $\mathbf{f} = \mathbf{b} + \mathbf{s}_l$, with the signal $\mathbf{s}_l$ centered at location l, $l \in \{1, \cdots, L\}$. We shall model signal location uncertainty with a pmf $p_{\mathbf{R}}(l)$ on the location l. Our observer or decision strategy will detect the presence or absence of the signal in the data $\mathbf{g}$ and, if a signal is detected, it will report a location $l(\mathbf{g})$ where it deems the signal to be present. If the true location of the signal falls within a tolerance region $T(l(\mathbf{g}))$ about the reported location $l(\mathbf{g})$, we will say that the observer has correctly localized the signal. Note that the inclusion of a tolerance region (typically a radius about the reported location) is an inherent part of a detection-localization task, and any FOM is dependent on the size of the tolerance region.

The test statistic is given by

$$t(\mathbf{g}) = \max_{l \in \{1,\cdots,L\}} \sum_{j \in T(l)} \frac{p(\mathbf{g}|\mathbf{b}+\mathbf{s}_j) p_{\mathbf{R}}(j)}{p(\mathbf{g}|\mathbf{b})} \tag{1}$$

with $l(\mathbf{g})$ being the location at which $t(\mathbf{g})$ is maximum. Note that Eq.(1) takes into account search tolerance. Also, this equation applies to a case of a discrete object and image, but can be generalized [1] to the realistic case of a continuous object and discrete image. One compares $t(\mathbf{g})$ to τ and decides signal present at location $l(\mathbf{g})$ if $t(\mathbf{g}) > \tau$ and signal absent if $t(\mathbf{g}) < \tau$.

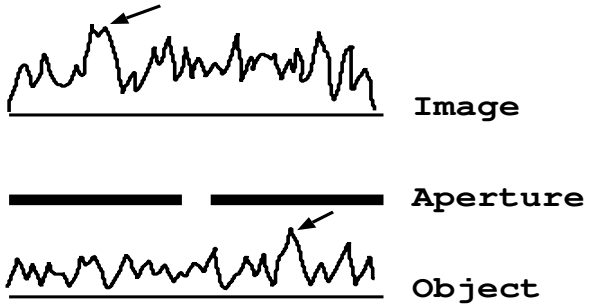

Fig. 1. Pinhole imaging system. The object is one sample from an ensemble with correlated backgound noise and variable signal location. The arrows indicate the signal location in object and image spaces.

Given the test statistics and reported locations, one can calculate the correct localization fraction CLF, which is the probability that a signal is correctly reported and localized given that it is present, as well as the FPF. By sweeping τ, one generates the LROC curve, a plot of CLF vs FPF. The area under the LROC curve, ALROC, is considered a FOM for the localization-detection problem. The decision strategy above is ideal in that no strategy can yield a greater ALROC and is also optimal in several other senses [1]. We refer to the decision strategy above as the "optimal LROC observer", an ideal observer for the detection-localization task.

To actually calculate ALROC, we use a Monte-Carlo (MC) procedure: For a given tolerance and aperture size, and with the signal absent or at one of its many locations, we generate many realizations of $\mathbf{g}$ and calculate $t(\mathbf{g})$ for each $\mathbf{g}$. Histograms of

$t(\mathbf{g})$ can be used [1] to generate the LROC curve and numerical integration used to obtain ALROC.

III. Aperture Optimization Experiments

We apply our optimal LROC observer to the problem of aperture optimization. We generated preliminary results using the 1-D unit-magnification pinhole system shown in Fig.1. The aperture has a binary transmission. The image $\mathbf{g} = H\mathbf{f} + \mathbf{n}$ where $\mathbf{n}$ is a data noise realization and H models aperture imaging via a simple convolution operation. Geometric and exposure time factors could be included in H, but we set these to unity without loss of generalization.

In the first experiment, we considered a 64-pixel object of fixed uniform background of intensity 10. The signal was triangular and of width = height = 5 units and could appear at any location (except for a few edge pixels) with equal probability. The data noise model is Poisson, so that the measurement model is given by $\mathbf{g}|\mathbf{f} \sim \text{Poisson}(H\mathbf{f})$. With this model, we can write $t(\mathbf{g})$ analytically as

$$t(\mathbf{g}) = \max_{l\in\{1,\cdots,L\}} \sum_{j\in T(l)} p_{\mathbf{R}}(j) \prod_m \left(\exp(-[H\mathbf{s}_j]_m)\left(1+\frac{[H\mathbf{s}_j]_m}{[H\mathbf{b}]_m}\right)^{g_m}\right)$$

where g_m is the count number in the mth image element.

We used the MC procedure to calculate ALROC and AROC vs aperture size as seen in Fig. 2. The optimal aperture for detection only is no aperture, as seen by the top curve in Fig. 2, which rises monotonically with aperture width. By adding a localization task, one expects a finite aperture to help localize the signal even though fewer counts are received. The LROC curves in Fig. 2 indeed show this, with an optimal aperture width of about 3 pixels at the smallest tolerance. Performance degrades (the curves get lower) as more precise localization is demanded, as one would expect.

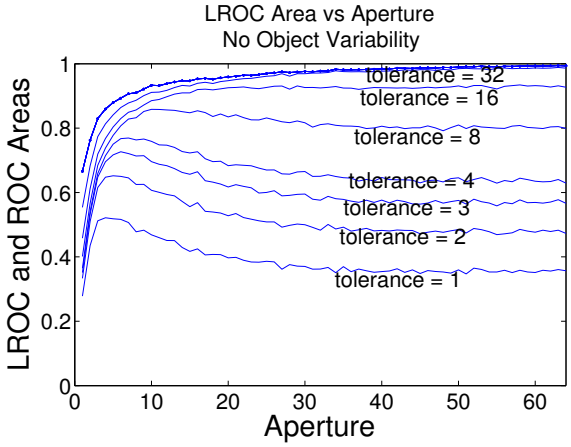

Fig. 2. ALROC versus aperture width for case of fixed background but variable signal location. The tolerance distances are indicated on each curve. The top curve corresponds to infinite tolerance (no localization) and is thus the AROC vs aperture curve.

In the second experiment, we explored the effects of background variability (BV). To a 32-pixel version of the objects considered in the first experiment, we added zero-mean correlated noise of standard deviation 2.2 and correlation length 6 pixels, obtained by sampling a stationary noise process whose power spectrum had a low-pass triangular shape. This yields a BV with covariance $\mathbf{K_b}$. Fig.1 shows a realization of a noisy object and its image.

One would again like to use the Poisson measurement model, but for the case of BV, this results in intractable expressions for the data likelihoods in Eq.(1). As a good approximation, we use an artificial measurement model $\mathbf{g}|\mathbf{f} \sim \mathcal{N}(H\mathbf{f}, \text{diag}(H\boldsymbol{\mu}_\mathbf{f}))$, where $\boldsymbol{\mu}_\mathbf{f}$ is the mean (over BV) object. With this measurement model, the first two moments of the data, $\bar{\mathbf{g}} = H\boldsymbol{\mu}_\mathbf{f}$ and $\mathbf{K_g} = \text{diag}(H\boldsymbol{\mu}_\mathbf{f}) + H\mathbf{K_b}H^T$, remain unchanged from the Poisson case. Now, one can write a complicated but easily evaluated analytical expression for $t(\mathbf{g})$ and apply the optimal LROC observer. We can again use the MC procedure to generate the ALROC and AROC vs. Aperture Width plots shown in Fig. 3. At small tolerance, there is again a performance drop and optimal aperture width (about 2.5 pixels at the smallest tolerance.) We expected a peak in the AROC (topmost) curve for pure detection with BV and signal-location unknown [3], but these preliminary results appear to indicate that no aperture is best even with BV.

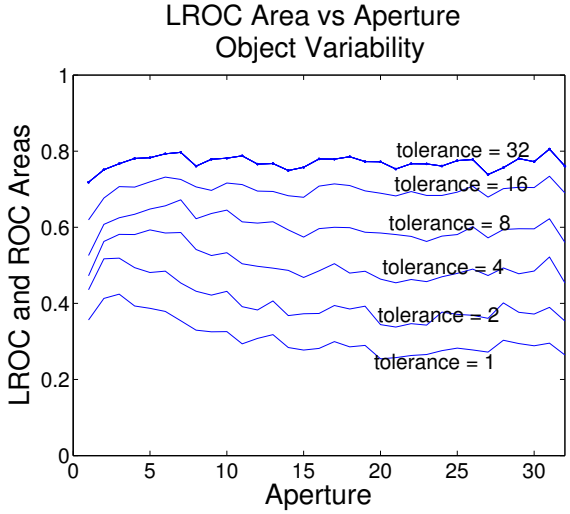

Fig. 3. ALROC versus aperture width for case of statistically variable background but variable signal location. The tolerance distances are indicated on each curve. The top curve (tolerance=32) corresponds to infinite tolerance (no localization) since the object and image are 32 pixels in length. The top curve is thus the AROC vs aperture curve.

IV. Discussion

We applied our new detection and localization ideal observers to aperture optimization and showed how the inclusion of localization changes the optimized imaging system. These results are preliminary and we intend to greatly extend them to the 2-D case and to more realistic measurement models for the case of background variability. Even for this simple problem, evaluation of the likelihood ratios in $t(\mathbf{g})$ via analytical expressions becomes quickly intractable for many cases of interest. We can use MCMC methods [4], [3] or other sampling methods to surmount this problem, however. Armed with such methods, we may be able to address the optimization of imaging systems more complex than the simple planar pinhole system used here.

References

[1] P. Khurd and G. Gindi, "Decision strategies that maximize the area under the LROC curve," *IEEE Trans. Med. Imaging*, vol. 24, no. 12, pp. 1626–1636, Dec. 2005.

[2] K. J. Myers, J. P. Rolland, R. F. Wagner, and H. H. Barrett, "Aperture optimization for emission imaging: Effect of a spatially varying background," *J. Optical Soc. America A*, vol. 7, no. 7, pp. 1279–1293, July 1990.

[3] S. Park, E. Clarkson, M. A. Kupinski, and H. H. Barrett, "Efficiency of the human observer detecting random signals in random backgrounds," *J. Optical Soc. America A*, vol. 22, no. 1, pp. 3–16, Jan. 2005.

[4] M. A. Kupinski, J. W. Hoppin, E. Clarkson, and H. H. Barrett, "Ideal-observer computation in medical imaging with use of Markov-chain Monte Carlo techniques," *J. Optical Soc. America A*, vol. 20, no. 3, pp. 430–438, March 2003.